Cytokine 123 (2019) 154745

Contents lists available at ScienceDirect

Cytokine

journal homepage: www.elsevier.com/locate/cytokine

Short-term RANKL exposure initiates a neoplastic transcriptional program in the basal epithelium of the murine salivary gland

Lan Hai[a,b,1], Maria M. Szwarc[a,1], David M. Lonard[a], Kimal Rajapakshe[a], Dimuthu Perera[a], Cristian Coarfa[a], Michael Ittmann[c], Rodrigo Fernandez-Valdivia[d], John P. Lydon[a,*]

[a] Department of Molecular and Cellular Biology, Baylor College of Medicine, Houston, TX, USA
[b] Reproductive Medicine Center of Henan Provincial People's Hospital, Zhengzhou, Henan Province, PR China
[c] Department of Pathology, Dan L. Duncan Comprehensive Cancer Center, Baylor College of Medicine, Houston, TX, USA
[d] Department of Pathology, Wayne State University School of Medicine Detroit, MI, USA

ARTICLE INFO

Keywords:
Mouse
RANKL
Salivary gland
Tumor
Transcriptome
RNA-seq

ABSTRACT

Although salivary gland cancers comprise only ~3–6% of head and neck cancers, treatment options for patients with advanced-stage disease are limited. Because of their rarity, salivary gland malignancies are understudied compared to other exocrine tissue cancers. The comparative lack of progress in this cancer field is particularly evident when it comes to our incomplete understanding of the key molecular signals that are causal for the development and/or progression of salivary gland cancers. Using a novel conditional transgenic mouse (*K5:RANKL*), we demonstrate that Receptor Activator of NFkB Ligand (RANKL) targeted to cytokeratin 5-positive basal epithelial cells of the salivary gland causes aggressive tumorigenesis within a short period of RANKL exposure. Genome-wide transcriptomic analysis reveals that RANKL markedly increases the expression levels of numerous gene families involved in cellular proliferation, migration, and intra- and extra-tumoral communication. Importantly, cross-species comparison of the *K5:RANKL* transcriptomic dataset with The Cancer Genome Atlas cancer signatures reveals the strongest molecular similarity with cancer subtypes of the human head and neck squamous cell carcinoma. These studies not only provide a much needed transcriptomic resource to mine for novel molecular targets for therapy and/or diagnosis but validates the *K5:RANKL* transgenic as a preclinical model to further investigate the *in vivo* oncogenic role of RANKL signaling in salivary gland tumorigenesis.

1. Introduction

Representing 3–6% of oropharyngeal cancers [1–4], salivary gland cancers are a rare and heterogeneous tumor type with at least 24 histologic subtypes of the malignant tumor class [3]. Although rare, salivary gland malignancies pose a significant public health concern as patients at advanced-stage have a poor prognosis in terms of their long-term survival. Unlike cancers of related exocrine tissues, prognostic and therapeutic management of salivary gland malignancies has not substantially improved in decades. For advanced tumors, radical surgical resection with subsequent adjuvant post-operative radiotherapy is usually the only treatment option [2,4]. Apart from facial disfigurement along with nerve damage that can occur with some surgeries (*i.e.* parotidectomy), sequelae from radiotherapy—xerostomia (dry mouth), taste loss, muscositis with recurrent oral infections, trismus, radiation caries, osteoradionecrosis, and dysphagia—can significantly reduce a patient's quality of life [5–7]. Because of their therapeutic ineffectiveness, current chemotherapeutic protocols are frequently repurposed for palliative rather than curative purposes for those patients with advanced-stage disease [2,8,9]. With limited therapeutic options currently available, the consensus in the field is that significant advancements in this area must come from the development of new targeted therapies [10–13]. Therefore, new oncogenic drivers and their downstream mediators that initiate and/or promote salivary gland tumorigenesis must be identified to achieve this goal.

A member of the tumor necrosis factor (TNF) superfamily of cytokines, receptor activator of NF-kB ligand (RANKL) signals through its receptor, RANK [14–16]. Although RANKL and RANK interact as transmembrane homotrimers, RANKL can also act on RANK through its cleaved ectodomain [17]. Engagement of RANKL with its receptor

* Corresponding author.
E-mail address: jlydon@bcm.edu (J.P. Lydon).
[1] Equal contribution (co-first authors).

https://doi.org/10.1016/j.cyto.2019.154745
Received 22 May 2019; Accepted 5 June 2019
Available online 18 June 2019
1043-4666/

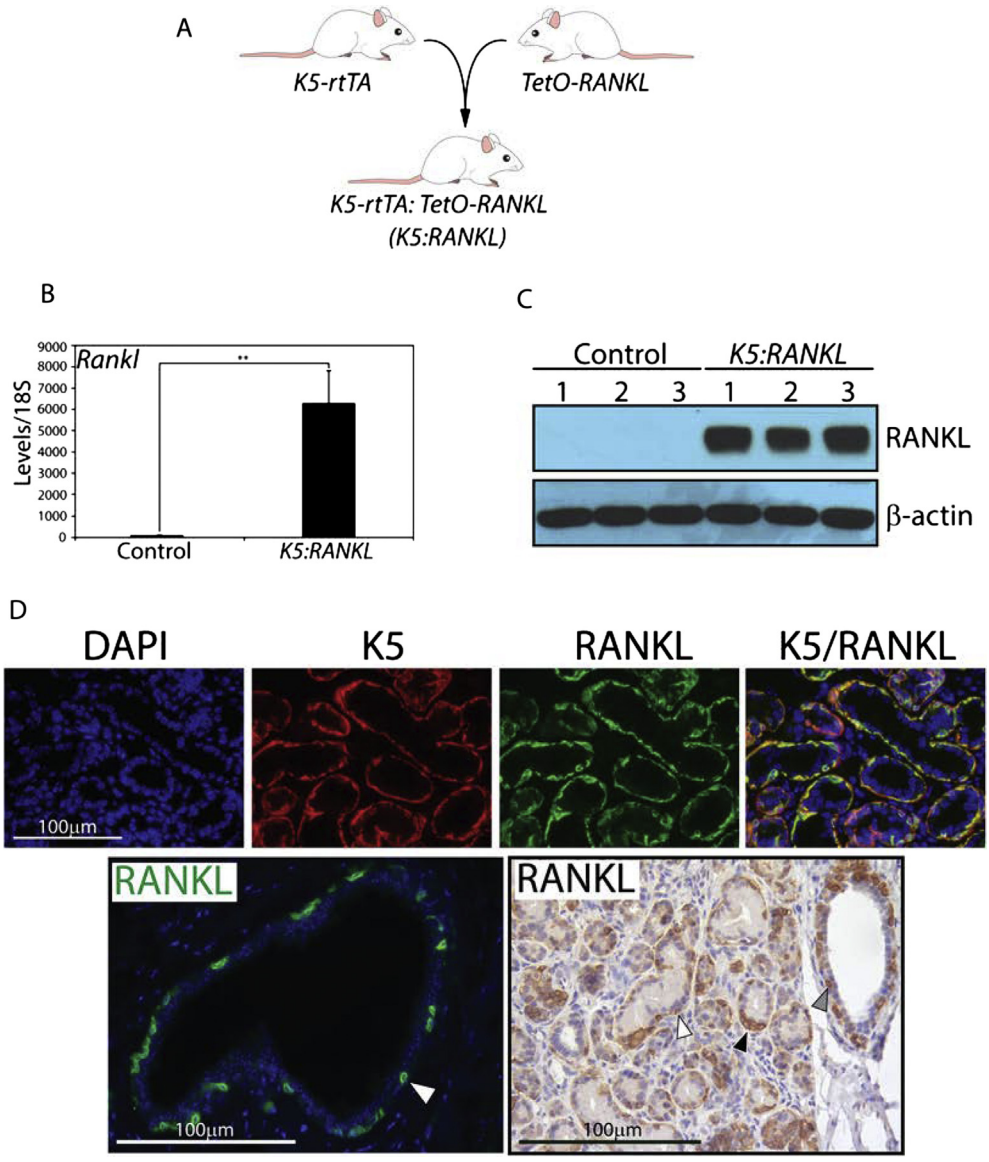

Fig. 1. Generation and characterization of the *K5:RANKL* bigenic mouse. (A) Breeding scheme to generate the *K5:RANKL* bigenic; the *K5-rtTA* and *TetO-RANKL* transgenic mice have been described [43–45]. (B) Quantitative real time PCR analysis shows that *Rankl* (*Tnfsf11*) mRNA levels are significantly increased in salivary gland tissue of adult *K5:RANKL* mice administered doxycycline for 5-days as compared to similarly treated monogenic control siblings (RNA pooled from five mice per genotype and analysis performed in triplicate). (C) Western immunoblot analysis confirms significant induction of RANKL protein in the salivary glands of *K5:RANKL* mice that were treated with doxycycline for 5-days; β-actin serves as a loading control. Each lane (lanes 1–3) represents salivary gland protein isolate pooled from three mice per genotype (nine mice total per genotype). (D) Top panels: dual immunofluorescence for K5 and RANKL spatial expression in *K5:RANKL* salivary gland tissue demonstrates coincident expression of both proteins. Left bottom panel shows immunofluorescence detection of RANKL expression in basal epithelial cells of an interlobular salivary gland duct (white arrowhead). Right bottom panel shows immunohistochemical detection of RANKL expression in basal epithelial cells in ductal and mucinous acini of the *K5:RANKL* salivary gland (gray and white arrowheads respectively); black arrowhead points to abnormal accumulation of RANKL positive basal epithelial cells. Scale bars denote 100 μm.

results in recruitment of TNF-receptor associated factors (TRAFs) to the cytoplasmic region of RANK, which triggers induction and/or activation of distinct signaling cascades in a cell-context dependent manner [18]. Numerous studies have demonstrated that unscheduled activation of the RANKL/RANK signaling axis drives a plethora of clinicopathologies, including cancers; reviewed in [19]. In the case of the mammary gland, a tubuloacinar exocrine tissue like the salivary gland, aberrant RANKL/RANK signaling underpins proliferative, invasive, migratory, and metastatic colonization properties of tumor cells by regulating a broad array of cellular responses, which include (but are not limited to) the execution of the epithelial-mesenchymal transition (EMT) program, enlarging the cancer stem cell population, and recruiting infiltrating tumor associated macrophages to the tumor microenvironment to enable neoplastic expansion, invasion, and metastasis [19–21].

In the case of human head and neck cancers, aberrant RANKL/RANK signaling has been linked to a number of oropharyngeal subtypes, particularly oral carcinomas [22–31]. Synthesized and secreted from oral squamous cell carcinomas, RANKL (as a paracrine signal) promotes osteolytic invasion of the mandibular bone [29–31], similar as in bone metastasis by other RANKL dependent cancers [14,32–35]. Recently, immunohistochemical studies have shown that the expression of RANKL and RANK is significantly higher in human salivary gland carcinomas as compared to adenomas [36]. Importantly, significant expression of RANKL and RANK was observed in salivary duct carcinomas and mucoepidermoid carcinomas [36], the latter are the most common malignancy type of the salivary gland [37–41].

Using conventional mouse transgenics, we previously demonstrated that RANKL expression targeted to the salivary gland epithelium results in malignancies with a prevalent mucoepidermoid histopathology [42]. While these studies provide functional support for a causal role for aberrant RANKL/RANK signaling in salivary gland tumor initiation and progression, the early molecular signals that mediate this tumorigenic response were not addressed. To address this issue, studies described herein used transcriptomic analysis of early neoplastic salivary gland tissues derived from a new bi-transgenic mouse model that enables short-term RANKL expression in cytokeratin 5 (K5)-positive basal epithelial cells following doxycycline administration in the adult.

2. Materials and methods

2.1. Generation of the K5:RANKL bigenic

The cytokeratin 5-reverse tetracycline transactivator (*K5-rtTA*)

Table 1
List of murine Taqman expression assays used in these studies.

Gene	ID	Catalog number
Aqp5	11,830	Mm00437578_m1
Amy1	11,722	Mm00651524_m1
Ccl8	20,307	Mm01297183_m1
Ccl9	20,308	Mm00441260_m1
Ccr1	12,768	Mm00438260_s1
Cldn22	75,677	Mm04209227_sH
Clec4n	56,620	Mm00490934_m1
Ctsk	13,088	Mm00484039_m1
Cxcl11	56,066	Mm00444662_m1
Dcpp1	13,184	Mm03019597_gH
Elf5	13,711	Mm00468732_m1
Esp8	100,126,778	Mm04243104_m1
Esp18	100,126,774	Mm04279607_m1
Fscn1	14,086	Mm00456046_m1
Krt17	1667	Mm00495207_m1
Mmp12	17,381	Mm00500554_m1
Muc19	239,611	Mm01306462_m1
Nfkb2	18,034	Mm00479807_m1
Postn	50,706	Mm01284919_m1
Prom2	192,212	Mm00617472_m1
Pthrp/Pthlh	19,227	Mm00436057_m1
Relb	19,698	Mm00485664_m1
Relt	320,100	Mm00723872_m1
Scgb2b26	110,187	Mm01254729_m1
Smr3a	20,599	Mm01964237_s1
Sox8	20,681	Mm00803422_m1
Spp1	20,750	Mm00436767_m1
Tfec	22,797	Mm01161234_m1
Tnfaip2	21,928	Mm00447578_m1
Tnfaip3	21,929	Mm00437121_m1
Tnfrsf4	22,163	Mm00442039_m1
Tnfrsf8	21,936	Mm00437140_m1
Tnfrsf1b	21,938	Mm00441889_m1
Tnfrsf11 (Rankl)	21,943	Mm00441906_m1
Tnfrsf11a (Rank)	21,934	Mm00437132_m1
Traf1	22,029	Mm00493827_m1
18S rRNA	Thermo Fisher Scientific Inc.: 4352930E	

transgenic mouse was purchased from The Jackson Laboratory, Bar Harbor, ME (JAX Mice Stock number: 017519; allele type: *Tg(KRT5-rtTA)T2D6Sgkd/J*). As described previously [43,44], the *K5-rtTA* transgenic mouse in the *FVB/NJ* inbred strain carries the bovine keratin 5 (*KRT5*) promoter, which drives expression of a nuclear localized *rtTA* gene. The *K5-rtTA* transgenic mouse enables the inducible expression of genes in K5 positive basal epithelial cells when administered doxycycline. The generation and characterization of our *TetO-RANKL* responder transgenic mouse was previously described [45]. Crossing the *K5-rtTA* effector transgenic with our *TetO-RANKL* responder transgenic generated the bigenic *K5-rtTA: TetO-RANKL* mouse (abbreviated *K5:RANKL* hereon (Fig. 1A)). The *K5:RANKL* bigenic mouse was designed so that doxycycline in the food and water will induce transgene-derived RANKL expression. To induce *RANKL* transgene expression in the *K5:RANKL* bigenic, adult (8–9 week old) mice (and monogenic *TetO-RANKL* control siblings) were switched to rodent chow containing doxycycline at 200 mg/kg (Bio-Serv, Flemington, NJ (#53888)) and to water containing 0.2% doxycycline (Takara BIO Inc., Mountain View, CA (#631311)) supplied in light protected bottles [45–47]. To reduce taste aversion, doxycycline fortified water was supplemented with 5% sucrose; doxycycline-supplemented water was changed every 3 days to maintain induction potency.

Mice used in these experiments were housed and maintained in an AAALAC accredited *vivarium* at Baylor College of Medicine. In temperature-controlled mouse rooms (22 ± 2 °C) with a 12-hour lights-on:12-hour lights-off photocycle, mice were fed irradiated Tekland global soy protein-free extruded rodent diet (Harlan Laboratories, Inc., Indianapolis, IN) with free access to fresh water. Experiments on mice were performed according to guidelines detailed in the Guide for the Care and Use of Laboratory Animals ("The Guide" (Eighth Edition 2011)), published by the National Research Council of the National Academies, Washington, D.C. (www.nap.edu). The Institutional Animal Care and Use Committee (IACUC) at Baylor College of Medicine prospectively approved all animal procedures used in this study.

2.2. Histological analysis

Fixed overnight in 4% paraformaldehyde, salivary gland normal (monogenic control) and *K5:RANKL* tumor tissue were processed for embedding in paraffin as reported [42]. Sections (5 μm) of salivary gland tissue and tumor were placed on Superfrost Plus glass slides (ThermoFisher Scientific, Waltham, MA) for immunohistochemical staining. Prior to staining, tissue sections were sequentially deparaffinized, rehydrated, and treated with an antigen unmasking solution [42]. After a blocking step, tissue and tumor sections were incubated with the appropriate primary antibody overnight. Primary antibodies used in these studies were: a rabbit polyclonal to human cytokeratin 5 (ab53121; Abcam Inc. (1:200), Cambridge, MA); a guinea pig polyclonal to bovine cytokeratin 8 + 18 (ab194130 (1:200); Abcam Inc.); a sheep polyclonal to 5-bromo-2-deoxyuridine (BrdU) (ab1893 (1:100); Abcam Inc.); a goat polyclonal anti-mouse RANKL (TRANCE; AF462 (1:200); R&D Systems, Minneapolis, MN); a rabbit polyclonal anti-human parathyroid hormone related peptide (PTHRP/PTHLH (parathyroid hormone like hormone); LS-B2325 (1:100); LifeSpan BioSciences Inc., Seattle, WA); a rabbit polyclonal anti-human secreted phosphoprotein 1 (SPP1 (osteopontin); ab8448; Abcam Inc.); and a goat polyclonal anti-mouse periostin (POSTN; AF2955 (1:100); R&D Systems). Following incubation with primary antibody, sections were incubated with the appropriate horseradish peroxidase conjugated secondary antibody (Vector laboratories Inc., Burlingame, CA) for 1 h at room temperature followed by incubation with the R.T.U Vectastain Universal ABC reagent (Vector laboratories Inc.) for 30 min at room temperature. Immunopositivity was visualized *in situ* through incubation with 3, 3′-diaminobenzidine (DAB, Vector laboratories Inc.); slides were lightly stained with hematoxylin for contrast. Following a stepwise dehydration process, slides with stained sections were mounted with coverslips using permount solution (Fisher Scientific Inc. (SP15-500)).

For BrdU immunohistochemical and immunofluorescence detection, mice received an intraperitoneal injection of BrdU (10 mg/ml; Amersham Biosciences Corporation, Piscataway, NJ) at a dose of 1 mg BrdU/20 g body weight two hours prior to euthanasia. For immunofluorescence detection, the following Alexa Fluor-conjugated secondary antibody combinations were used: Alexa Fluor 488 goat anti-rabbit IgG (A-11034) and Alexa Fluor 594 goat anti-guinea pig IgG (A-11076) were used to detect K5 and K8 + K18 respectively. Alexa Fluor 488 donkey anti-goat IgG (A-11055) and Alexa Fluor 546 donkey anti-sheep IgG (A-11016) were used to detect RANKL and BrdU respectively. Alexa Fluor-conjugated secondary antibodies were obtained from ThermoFisher Scientific Inc. Stained slides were mounted with coverslips using Vectashield mounting medium with DAPI (Vector Laboratories Inc., Burlingame, CA (H-1200)). Digital images of immunostained salivary gland tissue and tumor sections were captured using a color chilled AxioCam MRc5 digital camera attached to a Carl Zeiss AxioImager A1 upright microscope (Zeiss, Jena, Germany). For data display purposes, captured images were digitally collated and annotated with Photoshop and Illustrator (version 6) software (Adobe Systems Inc., San Jose, CA).

2.3. Quantitative real-time PCR analysis

Total RNA was extracted from salivary gland tissue and tumors using TRIzol reagent (ThermoFisher Scientific Inc.) before further purification with the RNeasy Plus Mini Kit (Qiagen Inc., Germantown Road, MD). Purified RNA was reversed transcribed into cDNA using the

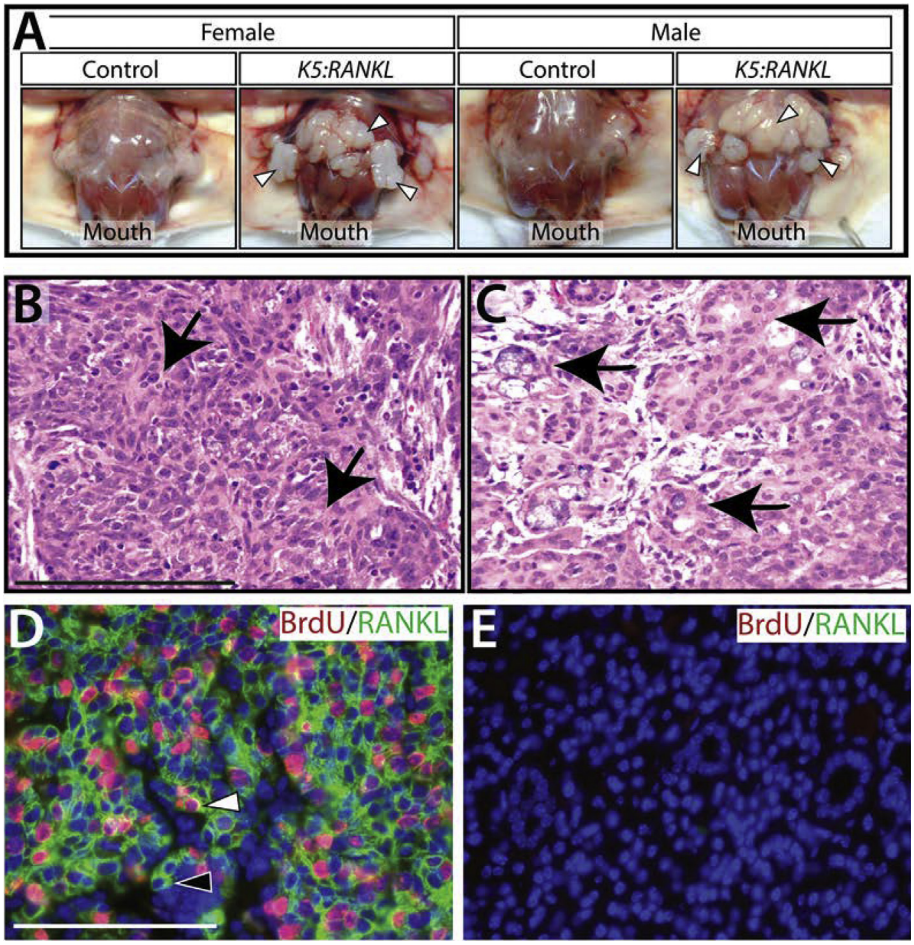

Fig. 2. Early morphological and neoplastic cellular changes in the *K5:RANKL* salivary gland with short-term RANKL expression. (A) Following two weeks of doxycycline administration, female and male *K5:RANKL* mice show clear evidence of gross morphological changes in their salivary glands (white arrowheads). Compared to controls, the *K5:RANKL* salivary gland neoplasms are significantly enlarged and ill-defined with a firm consistency. (B) Section stained with hematoxylin and eosin (H&E) from salivary gland neoplastic tissue of a *K5:RANKL* transgenic mouse shows evidence of squamous differentiation (arrows). (C) Focal glandular differentiation with areas of intracellular mucous is evident (arrows). (D) Dual immunofluorescence detection of BrdU (red) and RANKL (green) in a salivary gland tumor tissue section from a doxycycline-treated *K5:RANKL* mouse. Note the presence of tumor cells positive for RANKL and BrdU (white arrowhead) as well as tumor cells positive for RANKL alone (black arrowhead). (E) Dual immunofluorescence detection of BrdU and RANKL in salivary gland tissue derived from a similarly treated control mouse. Note the absence of immunopositivity for BrdU and RANKL in the tissue section. Scale bar (100 μm) in (B) applies to (C); scale bar (100 μm) in (D) applies to (E). (For interpretation of the references to colour in this figure legend, the reader is referred to the web version of this article.)

Superscript IV VILO Master Mix (ThermoFisher Scientific Inc.) before quantitative real-time PCR (qRT-PCR) amplification with the Applied Biosystems Step One Plus Real Time PCR System (ThermoFisher Scientific Inc.). Detailed information concerning the TaqMan gene expression assays used in these experiments is described in Table 1; 18S ribosomal RNA served as the internal control.

2.4. Transcriptomic profiling

As with our previous RNA-seq studies [48], RNA purity was evaluated with a NanoDrop spectrophotometer (ThermoFisher Scientific Inc.) and RNA integrity determined using a 2100 Bioanalyzer with RNA chips (Agilent Technologies, Santa Clara, CA). Only RNA preparations that scored a RNA integrity number (RIN) above 8 were used for RNA-seq. Libraries for mRNA sequencing were prepared with the TruSeq Stranded mRNA Library Prep kit (Illumina, San Diego, CA) from 250 ng of RNA. Quality analysis of libraries was performed using Agilent 4200 TapeStation with D1000 ScreenTape assays (Agilent Technologies). Libraries were pooled and then quantified by two methods: (1) on a 2100 Bioanalyzer with DNA chips using High Sensitivity DNA Kit (Agilent Technologies); and (2) with KAPA Library Quantification Kit for Illumina platforms (KAPA Biosystems, Wilmington, MA). Sequencing of mRNA libraries was performed on an Illumina NextSeq 500 platform at mid-output of paired-ended 75 base pair sequencing reads.

2.5. Analysis of sequenced mRNA

For initial analysis, pair-ended reads were aligned to the mouse genome (UCSC mm10) using open source STAR software [49] with NCBI RefSeq genes as the reference; gene expression was measured in read counts for each gene. The R package DESeq2 [50] was used to analyze the gene-based read counts to detect differentially expressed genes between monogenic control and *K5:RANKL* groups. The false discovery rate (FDR) of differentially expressed genes was estimated using the Benjamini and Hochberg method [51]; a FDR < 0.05 was considered statistically significant. Because of the large number of differentially expressed genes with a FDR < 0.05, a cut-off in absolute fold change $|FC| > 5$ and a sum of average counts of control and mutant sample > 100 was used for subsequent analysis. Raw mRNA sequencing data were deposited in NCBI/GEO with the super series accession code: GSE121954. Data were analyzed using the Database for Annotation, Visualization and Integrated Discovery (DAVID) version 6.8 Functional Annotation clustering tool and Kyoto Encyclopedia of Genes and Genomes (KEGG) Pathway Maps tool (http://david.ncifcrf.gov). For Gene Set Enrichment Analysis (GSEA; (http://software.broadinstitute.org/gsea/index.jsp)); mouse entrez gene identification numbers were matched to human homologs using their HomoloGene IDs.

2.6. Cross species analysis using the cancer genome atlas

For cross-species comparison analysis, mouse sequencing reads were first adaptor trimmed using TrimGalore software [52]. Trimmed reads were mapped to the mouse reference genome using the HISAT spliced alignment program [53]; transcript assembly and quantification were performed using StringTie software [53] against the Gencode gene model [54]. Gene expression (FPKM) was quantile normalized using R statistical software. Differentially expressed genes between *K5:RANKL* salivary gland tumor and corresponding control samples were determined using the parametric *t*-test with a p-value < 1.25. To

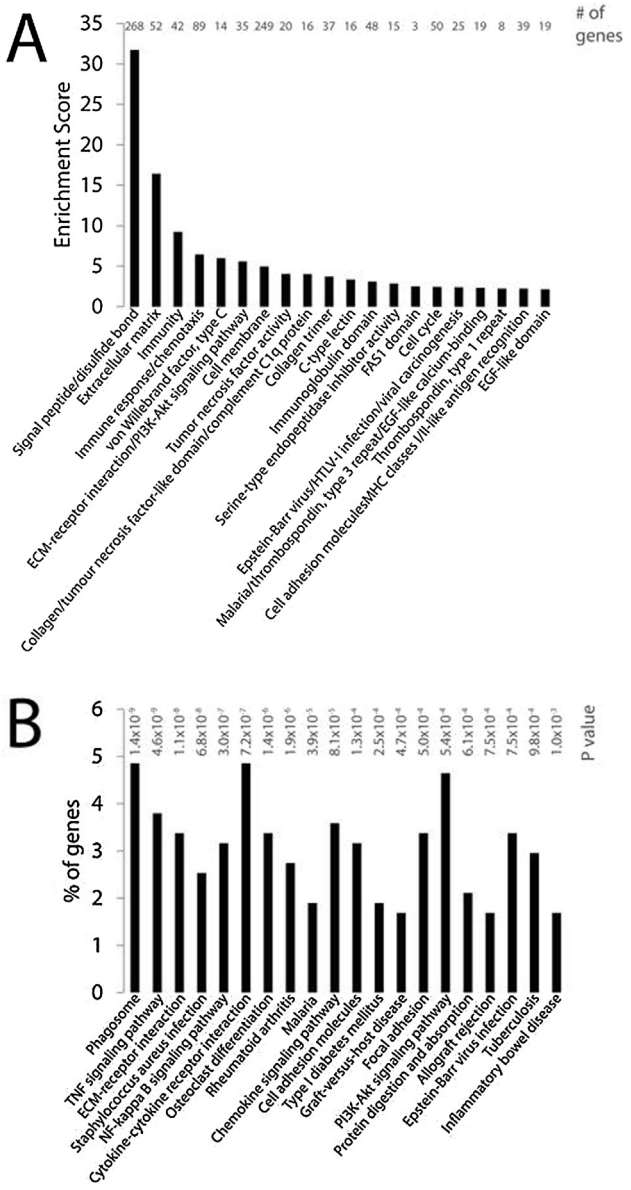

Fig. 3. Differentially expressed genes between *K5:RANKL* salivary gland tumors and control salivary gland tissue analyzed by DAVID. (A) DAVID functional annotation clustering analysis for enrichment of differentially expressed genes in functionally-related gene groups/gene ontology terms. The enrichment score is based on the EASA score of each term. (B) DAVID KEGG pathway analysis of biological/signaling pathways enriched in the differentially expressed gene dataset between *K5:RANKL* and control salivary gland group.

compare differentially expressed genes in the *K5:RANKL* tumor dataset with multiple human cancers profiled by The Cancer Genome Atlas (TCGA), GSEA was applied to both up- and down-regulated genes in the *K5:RANKL* tumor dataset against rank files from multiple cohorts of TCGA human cancers. Results were ranked using a similarity score rewarding matching direction for normalized enriched scores for up- and down- regulated genes [55]. Normalized enrichment scores (NES) for TCGA human cancer gene signatures and for our *K5:RANKL* tumor dataset were displayed in a circular combined format using Circos software (http://circos.ca/) [56].

2.7. Western immunoblot analysis

Protein was isolated from salivary gland tissue and tumors and Western immunoblotting was conducted as previously reported [47]. Before transfer to polyvinylidene difluoride membranes (Bio-Rad Laboratories, Hercules, CA), protein (20 μg) was separated by electrophoresis on a 4–15% gradient sodium dodecyl sulfate-polyacrylamide gel. The following primary antibodies (at 1:1000 dilution) were used: goat polyclonal anti-mouse RANKL (AF462; R&D Systems) and a mouse monoclonal anti-human β-actin (Sigma-Aldrich, St. Louis, MO; A1978). After incubation with the appropriate secondary antibody, immunopositive bands were visualized using the SuperSignal West Pico Chemiluminescent Substrate kit (ThermoFisher Scientific Inc.). To enable re-probing of the same membrane with different antibodies, membranes were stripped of primary and secondary antibodies using Restore Western Blot Stripping buffer ((#21059) ThermoFisher Scientific Inc.).

2.8. Statistical evaluation

As required, data are displayed as means ± standard deviation. The significance of the difference between groups was determined by two-tailed Student's *t* tests and one-way ANOVA with Tukey's *post-hoc* multiple range tests using the GraphPad and Instat statistical analysis tools (GraphPad software Inc., La Jolla, CA). Unless indicated otherwise, at least three independent replicates were used, and no samples were excluded from any study. A p-value < 0.05 was considered statistically significant; asterisks in histograms denote the level of significance: *$p < 0.05$; **$p < 0.01$; and ***$p < 0.001$.

3. Results

3.1. Short-term doxycycline administration induces RANKL expression in basal epithelial cells of the K5:RANKL salivary gland

For transcriptomic profiling described in these studies, the *K5:RANKL* bigenic mouse (Fig. 1A) was used to enable short-term induction of transgene-derived RANKL expression by doxycycline in a specific cell-type of the salivary gland (the K5 positive abluminal basal epithelial cell) at a predetermined age (9-weeks) and for a defined period of time (2-weeks). The above approach was feasible because: (a) RANK is ubiquitously expressed at low levels in the epithelial compartment of the mouse salivary gland [42]; and (b) the *TetO-RANKL* effector transgene has proven highly efficient in targeting RANKL expression specifically in response to doxycycline administration [45]. With just 5-days of doxycycline administration, *RANKL* was significantly induced at the RNA and protein level in salivary gland tissue of adult *K5:RANKL* mice (Fig. 1B, C); similarly treated monogenic *TetO-RANKL* control mice did not exhibit this induction (Fig. 1B, C). As expected, *K5:RANKL* mice without doxycycline in the food and water did not exhibit RANKL induction (data not shown). Immunohistochemical analysis showed that doxycycline-induced RANKL expression occurred in the K5 positive basal epithelial cell-type throughout the salivary gland (Fig. 1d). Before this immunohistochemical analysis, we confirmed that dual immunofluorescence detection of K5 and K8 + 18 clearly defines the abluminal basal and luminal epithelial cellular compartments respectively of the normal salivary gland duct (Supplementary Fig. 1).

3.2. The K5:RANKL salivary gland tumor exhibits a predominant mucoepidermoid histopathology in response to short-term RANKL exposure

By two weeks of doxycycline administration, both female and male adult *K5:RANKL* transgenic mice exhibit a swollen neck region that is texturally hard and irregular by palpation (Fig. 2A and Supplementary Fig. 2). The salivary gland phenotype was 100% penetrant (n = 30 *K5:RANKL* females and n = 20 *K5:RANKL* males (compared with an equal number of similarly treated control mice)) and occurred in the three major salivary glands in the majority of *K5:RANKL* mice examined. Similar to our recent report [42], the histopathology of both

Table 2
Top 50 genes upregulated in the *K5:RANKL* salivary gland tumor.

GENE SYMBOL	GENE ID	GENE NAME	K5:RANKL/CONTROL
Ccl20	20,297	chemokine (C-C motif) ligand 20	577.6
Alox12e	11,685	arachidonate lipoxygenase, epidermal	468.7
Abca13	268,379	ATP-binding cassette, sub-family A (ABC1), member 13	269.7
Dsg1a	13,510	desmoglein 1 alpha	215.4
Msln	56,047	mesothelin	176.0
Gm8909	667,977	predicted gene 8909	152.5
Hal	15,109	histidine ammonia lyase	144.4
Tnfsf11	**21,943**	**tumor necrosis factor (ligand) superfamily, member 11**	**127.7**
Eno1b	433,182	enolase 1B, retrotransposed	126.0
Calcb	116,903	calcitonin-related polypeptide, beta	116.7
Irg1	16,365	immunoresponsive gene 1	113.2
Fcgbp	215,384	Fc fragment of IgG binding protein	90.8
Plb1	665,270	phospholipase B1	87.9
H2-Ea-ps	100,504,404	histocompatibility 2, class II antigen E alpha, pseudogene	86.5
Slc30a2	230,810	solute carrier family 30 (zinc transporter), member 2	84.2
Alox15	11,687	arachidonate 15-lipoxygenase	83.7
Spp1	20,750	secreted phosphoprotein 1	79.6
Serpina3h	546,546	serine (or cysteine) peptidase inhibitor, clade A, member 3H	78.3
Gad1	14,415	glutamate decarboxylase 1	72.4
Spink5	72,432	serine peptidase inhibitor, Kazal type 5	65.2
Dsg1b	225,256	desmoglein 1 beta	64.0
Thbs4	21,828	thrombospondin 4	60.3
Plekhs1	226,245	pleckstrin homology domain containing, family S member 1	60.2
Sox8	20,681	SRY (sex determining region Y)-box 8	60.2
Mmp12	17,381	matrix metallopeptidase 12	59.6
Cd207	246,278	CD207 antigen	59.5
Mmp9	17,395	matrix metallopeptidase 9	59.5
H2-Q1	15,006	histocompatibility 2, Q region locus 1	57.6
Sectm1a	209,588	secreted and transmembrane 1A	57.0
Serpina3n	20,716	serine (or cysteine) peptidase inhibitor, clade A, member 3 N	54.3
Gdpd3	68,616	glycerophosphodiester phosphodiesterase domain containing 3	53.4
Tnfrsf11b	18,383	tumor necrosis factor receptor superfamily, member 11b (osteoprotegerin)	52.0
Fcamr	64,435	Fc receptor, IgA, IgM, high affinity	52.0
Adamts13	279,028	a disintegrin-like and metallopeptidase (reprolysin type) with thrombospond	48.9
Foxn1	15,218	forkhead box N1	48.1
Wnt7b	22,422	wingless-type MMTV integration site family, member 7B	47.6
Tnfaip2	21,928	tumor necrosis factor, alpha-induced protein 2	46.4
Cxcl11	56,066	chemokine (C-X-C motif) ligand 11	46.3
Gm1821	218,963	ubiquitin pseudogene	46.3
Serpina3i	628,900	serine (or cysteine) peptidase inhibitor, clade A, member 3I	44.8
Col8a1	12,837	collagen, type VIII, alpha 1	44.1
Cyp2a5	13,087	cytochrome P450, family 2, subfamily a, polypeptide 5	40.3
Aadac	67,758	arylacetamide deacetylase (esterase)	39.5
Ctsk	13,038	cathepsin K	39.1
Ccl9	20,308	chemokine (C-C motif) ligand 9	37.0
S100a14	66,166	S100 calcium binding protein A14	34.9
Gm8615	667,410	glucosamine-6-phosphate deaminase 1 pseudogene	34.7
Ccnb1ip1	239,083	cyclin B1 interacting protein 1	33.1
C920025E04Rik	667,803	RIKEN cDNA C920025E04 gene	32.9
Spib	272,382	Spi-B transcription factor (Spi-1/PU.1 related)	32.2

female and male *K5:RANKL* salivary gland neoplasms following 2-weeks of doxycycline administration was consistent with a high grade mucoepidermoid carcinoma with sparsely distributed mucinous cells and more frequently occurring epidermoid (squamoid) cells with pale to eosinophilic cytoplasm along with nondescript intermediate cells in varied proportions (Fig. 2B,C and Supplementary Fig. 3). Dual immunofluorescence detection of RANKL expression and BrdU incorporation revealed that tumor areas in the *K5:RANKL* salivary gland are highly proliferative and heterogeneous in terms of tumor cells that are double immunopositive for RANKL and BrdU or immunopositive for RANKL alone. However, approximately 35% of tumor cells are double positive for RANKL and BrdU, indicating a possible autocrine and/or paracrine signaling mode for RANKL action in this tumor tissue [42]. Not surprisingly, transgene-derived RANKL expression was detected in K5 positive basal cells in tissues other than the salivary gland (*i.e.* mammary gland, thymus, and skin (data not shown)). However, because of the short-term administration of doxycycline, the effects of transgene-derived RANKL expression in K5 positive basal cell types in other epithelial tissues was minimal with only marginal increased branching morphogenesis in the female mammary gland and a slight enlargement of the thymus in both sexes (data not shown).

3.3. Transcriptional reprogramming by RANKL drives salivary gland tumorigenesis

To identify downstream contributory signals that may underpin early neoplastic cellular changes in the *K5:RANKL* salivary gland, mRNA-seq analysis was performed using salivary gland tissue derived from *K5:RANKL* female mice and corresponding monogenic controls, which were administered doxycycline at 9-weeks of age for two weeks. Triplicate mRNA samples from *K5:RANKL* and control groups (n = 5 mice per replicate; 15 mice total per genotype) were sequenced at an average of 20 million read-pairs per sample. Using a FDR < 0.05 and a $|FC| > 5$ (and sum of control and *K5:RANKL* counts > 100), a total of 471 genes (375 up-regulated and 96 down-regulated) were differentially expressed between the *K5:RANKL* and control groups (Supplementary File 1); Tables 2 and 3 display the top 50 genes up- and down-regulated respectively. This degree of stringency was chosen to

Table 3
Top 50 genes downregulated in the *K5:RANKL* salivary gland tumor.

GENE SYMBOL	GENE ID	GENE NAME	*K5:RANKL*/CONTROL
BC018473	193,217	cDNA sequence BC018473	−564.7
Dcpp3	620,253	demilune cell and parotid protein 3	−89.6
Pgr	18,667	progesterone receptor	−74.1
Hapln4	330,790	hyaluronan and proteoglycan link protein 4	−62.2
Cldn22	75,677	claudin 22	−49.5
Crisp1	11,571	cysteine-rich secretory protein 1	−43.1
Bpifa2	19,194	BPI fold containing family A, member 2	−42.2
Nxpe4	244,853	neurexophilin and PC-esterase domain family, member 4	−41.6
Smr3a	20,599	submaxillary gland androgen regulated protein 3A	−41.0
Prb1	381,833	proline-rich protein BstNI subfamily 1	–33.8
Dnase1	13,419	deoxyribonuclease I	−31.1
Azgp1	12,007	alpha-2-glycoprotein 1, zinc	−28.3
St6galnac1	20,445	ST6 (alpha-N-acetyl-neuraminyl-2,3-beta-galactosyl-1,3)-N-acetylgalactosam	−26.3
Prpmp5	381,832	proline-rich protein MP5	−24.2
Ggh	14,590	gamma-glutamyl hydrolase	–22.9
2610507I01Rik	72,203	RIKEN cDNA 2610507I01 gene	−19.4
Amy1	11,722	amylase 1, salivary	−19.1
Rab6b	270,192	RAB6B, member RAS oncogene family	−18.9
Esp18	100,126,774	exocrine gland secreted peptide 18	−18.3
1700066N21Rik	73,471	RIKEN cDNA 1700066 N21 gene	−18.3
Shisa7	232,813	shisa family member 7	−16.1
Ret	19,713	ret proto-oncogene	−14.7
Lipo1	381,236	lipase, member O1	−14.2
Gm4736	114,600	predicted gene 4736	−13.7
H2-Eb1	14,969	histocompatibility 2, class II antigen E beta	−12.5
Mup6	620,807	major urinary protein 6	−11.8
Ttr	22,139	transthyretin	−11.5
Gprc6a	210,198	G protein-coupled receptor, family C, group 6, member A	−11.0
Fgf1	14,164	fibroblast growth factor 1	−10.9
Cst10	58,214	cystatin 10 (chondrocytes)	−10.3
Chia1	81,600	chitinase, acidic 1	−10.0
Agt	11,606	angiotensinogen (serpin peptidase inhibitor, clade A, member 8)	−10.0
B4galnt3	330,406	beta-1,4-N-acetyl-galactosaminyl transferase 3	−9.7
Rbm20	73,713	RNA binding motif protein 20	−9.6
9130230L23Rik	231,253	RIKEN cDNA 9130230L23 gene	−9.6
Tcea3	21,401	transcription elongation factor A (SII), 3	−9.2
AI463170	100,504,549	expressed sequence AI463170	−8.9
Isoc2b	67,441	isochorismatase domain containing 2b	−8.7
Unc5a	107,448	unc-5 netrin receptor A	−8.5
Atp6v1c2	68,775	ATPase, H + transporting, lysosomal V1 subunit C2	−8.4
Ttc25	74,407	tetratricopeptide repeat domain 25	−8.4
2310057J18Rik	67,719	RIKEN cDNA 2310057 J18 gene	−8.3
Esp8	100,126,778	exocrine gland secreted peptide 8	−8.2
4833423E24Rik	228,151	RIKEN cDNA 4833423E24 gene	−8.2
Insig1	231,070	insulin induced gene 1	−8.0
Rap1gap	110,351	Rap1 GTPase-activating protein	−7.9
Muc19	239,611	mucin 19	−7.9
Aldh3b2	621,603	aldehyde dehydrogenase 3 family, member B2	−7.8
Scgb2b26	110,187	secretoglobin, family 2B, member 26	−7.8
Gpr37l1	171,469	G protein-coupled receptor 37-like 1	−7.7

enable subsequent gene enrichment analysis. Differentially expressed genes analyzed with DAVID for functional enrichment and for enrichment in biological pathways cataloged in KEGG respectively revealed a significant representation in genes involved in signal peptide/disulfide bond, extracellular matrix (EM)-receptor interactions, immune response/chemotaxis, tumor necrosis factor signaling, NF-kB signaling, and osteoclast differentiation (Fig. 3 and Supplementary File 1). Collectively, these genes serve critical functions in neoplastic development and progression, including cellular proliferation, survival, promotion of EMT, migration, invasion into the tumor microenvironment, and metastasis. Validation at the transcript level of a selection of these differentially expressed genes is shown (Fig. 4 and Supplementary Fig. 4). In keeping with the established mediator role for RANKL [18,19], members of the NF-kB signaling cascade are significantly represented in the *K5:RANKL* tumor signature as well as pro-inflammatory cytokine/chemokine family members (Figs. 3, 4). Not surprisingly, many genes (*i.e.* amylase 1 (*Amy1*) and aquaporin 5 (*Aqp5*)) involved in normal salivary gland function are significantly down-regulated in the *K5:RANKL* salivary gland tumor compared to normal salivary gland tissue (Supplementary Fig. 4). Although salivary gland excrinopathy is predicted by the down-regulation in the expression of these genes, the *K5:RANKL* mice did not exhibit overt signs of salivary gland dysfunction (*i.e.* absence or reduced saliva).

3.4. The K5:RANKL salivary gland tumor is most closely related to human head and neck squamous cell carcinoma subtypes

To determine the translational significance of our molecular findings in the *K5:RANKL* salivary gland tumor, we assessed the degree of molecular similarity between our *K5:RANKL* tumor transcriptomic dataset with transcriptomic signatures of 25 human cancers profiled in the TCGA. Combined NES for all TCGA tumor development gene signatures and our *K5:RANKL* tumor dataset were visualized using Circos software (Fig. 5A [56]). Of the 25 human cancers analyzed, head and neck squamous cell carcinoma (HNSCC) subtypes were listed within the top four cancers—HNSC (mesenchymal subtype); kidney renal clear-cell carcinoma (KIRC); HNSC (basal); and HNSC (atypical)—that scored the closest molecular similarity to the *K5:RANKL* tumor transcriptomic

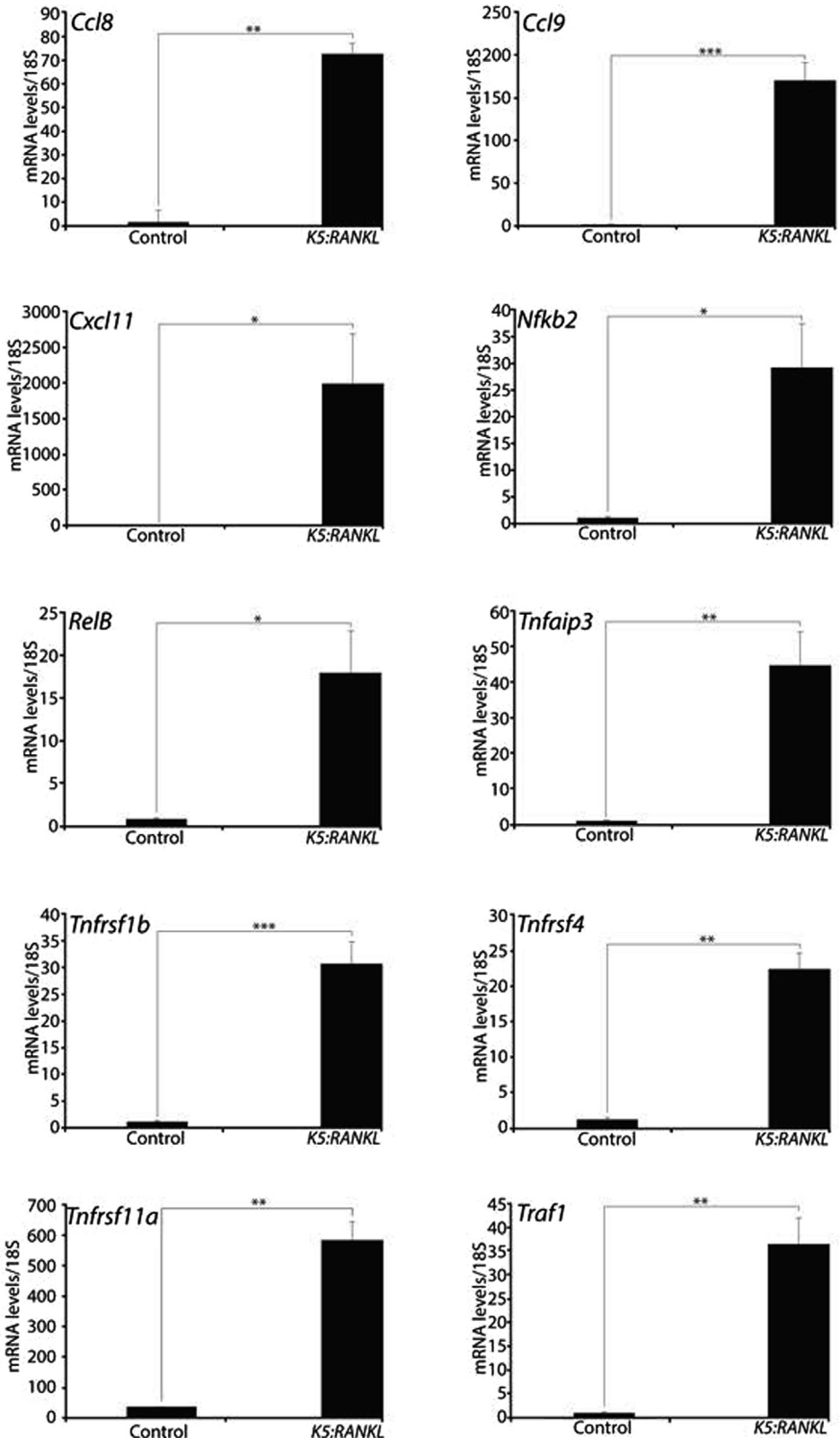

Fig. 4. Genes involved in chemokine, NFkB, and TNF signaling are significantly expressed in the *K5:RANKL* salivary gland tumor. Quantitative real-time PCR demonstrates that members of the chemokine/chemokine receptor (*i.e. chemokine (C-C motif) ligand 8 (Ccl8)*; *chemokine (C-C motif) ligand 9 (Ccl9)*; *C-C chemokine receptor type 1 (Ccr1)*; and *C-X-C motif chemokine 11 (Cxcl11))*; NFkB (*i.e. nuclear factor kappa B subunit 2 (Nfkb2)*; and *RelB proto-oncogene, Nfkb subunit (RelB))*; and TNF (*i.e. TNF alpha induced protein 3 (Tnfaip3)*; *TNF receptor superfamily member 1B (Tnfrsf1b)*; *TNF receptor superfamily member 4 (Tnfrsf4)*; *TNF receptor superfamily member 11a* (*Tnfrsf11a* (*Rank*)); and *TNF receptor associated factor 1 (Traf1))* signaling pathways are highly expressed in *K5:RANKL* salivary gland tumors. Data are represented as the average expression fold change relative to control group ± standard deviation (n = 4 mice per control and *K5:RANKL* groups).

signature (Fig. 5A,B). Many of the pathways enriched between the HNSC (mesenchymal) and our *K5:RANKL* tumor dataset are associated with tumor cell proliferation, migration, and metastasis (Fig. 5C and Supplemental File 2). All gene expression changes, which were selected from this gene list (Supplementary File 2), validated at the transcriptional level (Fig. 6). Using PTHRP, SPP1 and POSTN as examples from this gene list (Supplementary File 2), our immunohistochemical analysis confirmed significant expression of these three genes at the protein level in *K5:RANKL* salivary gland tumors as compared with control salivary gland tissue (Fig. 7).

4. Discussion

Advancement in the development of effective molecular diagnostics

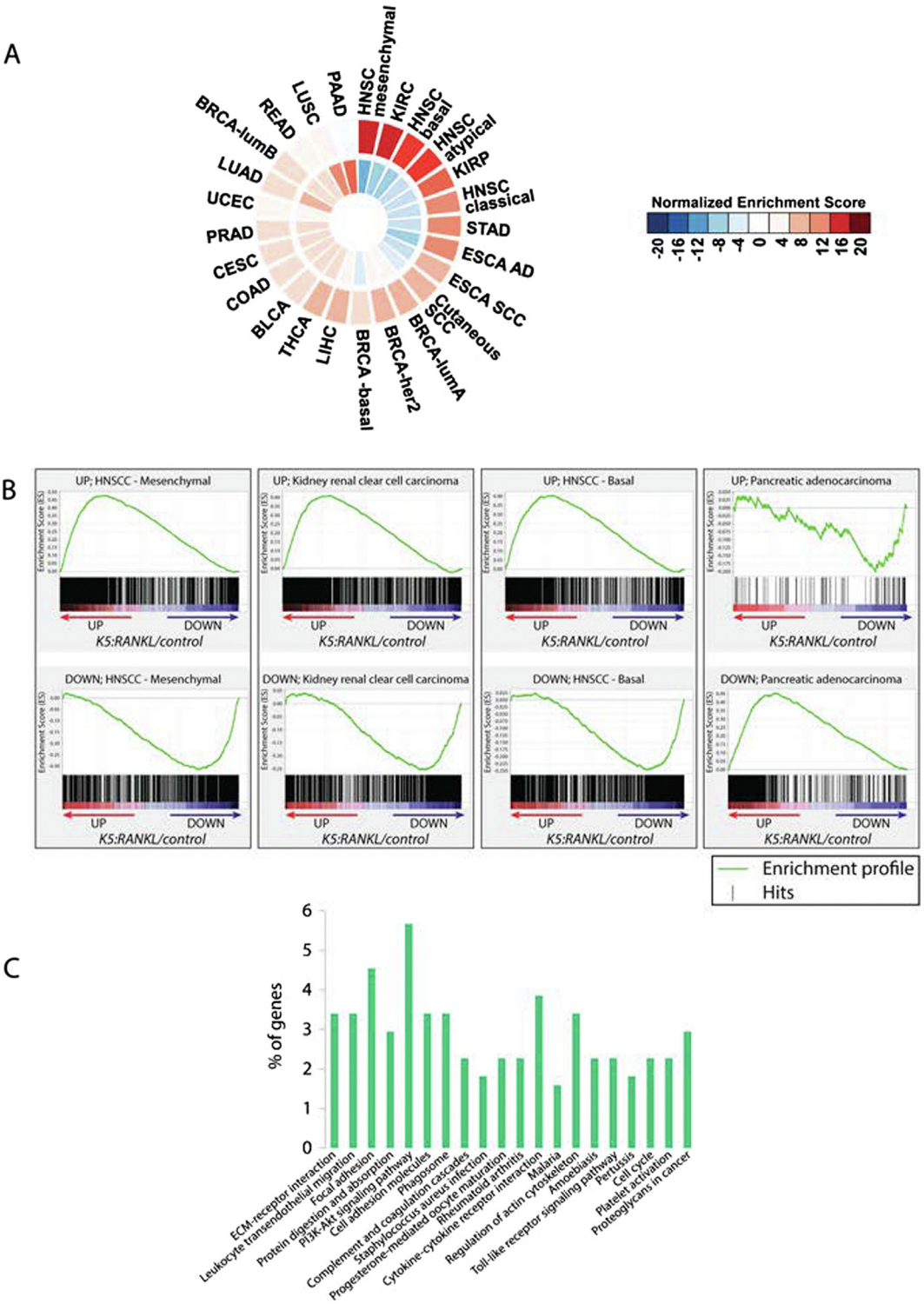

Fig. 5. The molecular signature of the *K5:RANKL* salivary gland tumor most closely resembles human head and neck squamous cell carcinoma subtypes. (A) Normalized enrichment scores for each of the 25 human cancer signatures compared to corresponding *K5:RANKL*/control were calculated. Cancer types were ranked by similarity to the *K5:RANKL* salivary gland tumor signature in descending order and in a clockwise direction on a Circos Plot. The outside ring displays enrichment of up-regulated transcripts while the inside ring shows the enrichment of down-regulated transcripts. Circular presentation of the data clearly shows that the *K5:RANKL* signature is most closely related to mesenchymal and basal subtypes of the head and neck squamous cell carcinoma (HNSCC). Note: Head and neck squamous cell carcinoma–mesenchymal subtype (HNSC-mesenchymal); kidney renal clear cell carcinoma (KIRC); kidney renal papillary cell carcinoma (KIRP); stomach adenocarcinoma (STAD); esophageal adenocarcinoma (ESCA AD); esophageal squamous cell carcinoma (ESCA SCC); cutaneous squamous cell carcinoma (SCC); breast cancer luminal A (lum A) subtype; breast cancer her2 subtype; breast cancer basal subtype; liver hepatocellular carcinoma (LIHC); thyroid carcinoma (THCA); bladder urothelial carcinoma (BLCA); colon adenocarcinoma (COAD); cervical squamous cell carcinoma and endocervical adenocarcinoma (CESC); prostate adenocarcinoma (PRAD); uterine corpus endometrial carcinoma (UCEC); lung adenocarcinoma (LUAD); breast cancer luminal B subtype (BRCA-lumB); rectum adenocarcinoma (READ); lung squamous cell carcinoma (LUSC); and pancreatic adenocarcinoma (PAAD). (B) Enrichment plots of the TCGA tumor datasets that most positively and inversely correlated with the *K5:RANKL* gene expression signature. (C) Pathway analysis by DAVID KEGG pathway tool of genes shared between the HNSCC GSEA datasets and the mouse *K5: RANKL* signature.

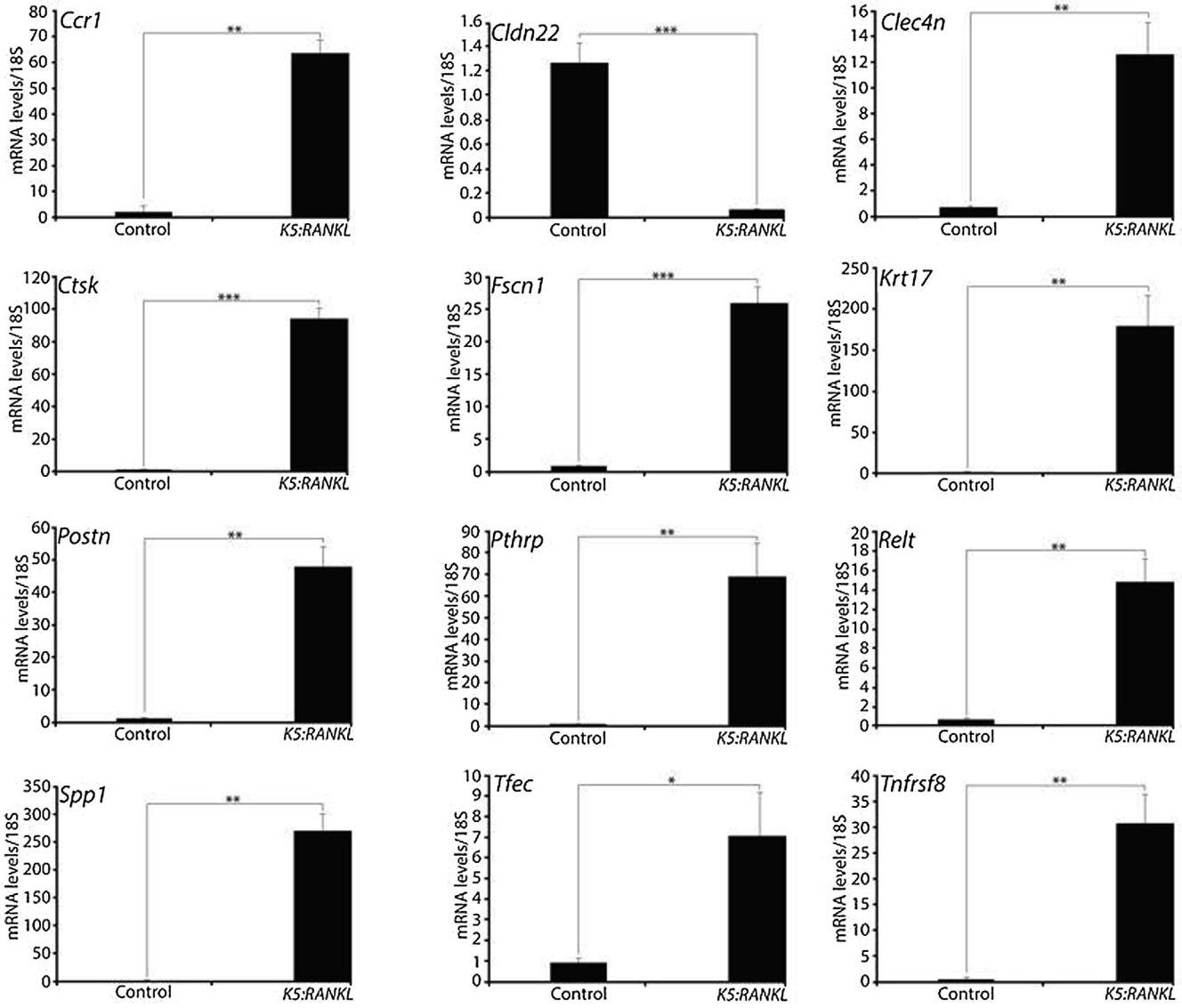

Fig. 6. Validation of gene expression changes in the *K5:RANKL* salivary gland tumor that are also changed in human head and neck squamous cell carcinomas. Quantitative real time PCR results show significant expression changes of genes (*i.e. C-C motif chemokine receptor 1 (Ccr1)*; *Claudin 22 (Cldn22)*; *C-type lectin domain family 4, member n (Clec4n)*; *Cathepsin K (Ctsk)*; *Fascin 1 (Fscn1)*; *Keratin 17 (Krt 17)*; *Periostin (Postn)*; *Parathyroid hormone related peptide (Pthrp)*; *Receptor expressed in lymphoid tissue (Relt)*; *Secreted phosphoprotein 1 (Spp1)*; *Transcription factor EC (Tfec)*; and *Tumor necrosis factor receptor superfamily member 8 (Tnfrsf8))* in the *K5:RANKL* salivary gland tumor that are also markedly changed in expression levels in human head and neck squamous cell carcinomas (Supplementary File 2). Data are represented as standard deviation of the average fold change (n = 4 mice per control and *K5:RANKL* groups).

and targeted therapeutics for the clinical management of salivary gland malignancies has been hampered by the limited availability of suitable experimental models, particularly *in vivo* models such as the mouse. As clearly demonstrated for cancers of other glandular tissues (*i.e.* the mammary gland), mouse models for these cancers have been successfully used not only for gaining essential insights into the molecular mechanisms that underpin all stages of tumor development and progression but also to test investigational and repurposed drugs as possible novel anti-neoplastic therapies.

In transgenic mouse studies described here, we demonstrate that targeting RANKL to K5 positive basal cells of the salivary gland epithelium elicits rapid tumorigenesis. The predominant histopathology of a high-grade mucoepidermoid carcinoma exhibited by these tumors is clinically significant as this tumor subtype is the most common salivary gland malignancy [40,41,57] and has recently been shown to express RANKL and RANK [36]. Moreover, patients with high-grade mucoepidermoid carcinomas have low survival rates and high morbidity following treatment due in part to tumor resistance to conventional platinum-based chemotherapy and ionizing radiation [58–60]. Recent studies have also shown that mucoepidermoid carcinomas express high basal levels of NFkB, which may contribute to their chemoresistance and radioresistance [58,60]. In the same studies, targeting NFkB signaling in a combined therapy protocol was shown to be effective in markedly reducing the resistance phenotype of human mucoepidermoid carcinoma cell lines in culture [58,60]. Because many activators and mediators of the NFkB pathway are markedly up-regulated in the salivary gland tumor of the *K5:RANKL* mouse (Figs. 3, 4 and Supplementary Table 1), this transgenic represents a potentially important preclinical model in which to test the efficacy of these new mechanism-based therapeutic approaches in an *in vivo* context.

Using the *K5:RANKL* mouse, together with genome-wide RNA profiling, we disclosed a complex transcriptomic signature that underlies salivary gland tumorigenesis in response to short-term RANKL exposure. Despite this complexity, gene set enrichment analysis and pathway analytics revealed a significant enrichment of transcriptional programs that exert important functions in cellular proliferation,

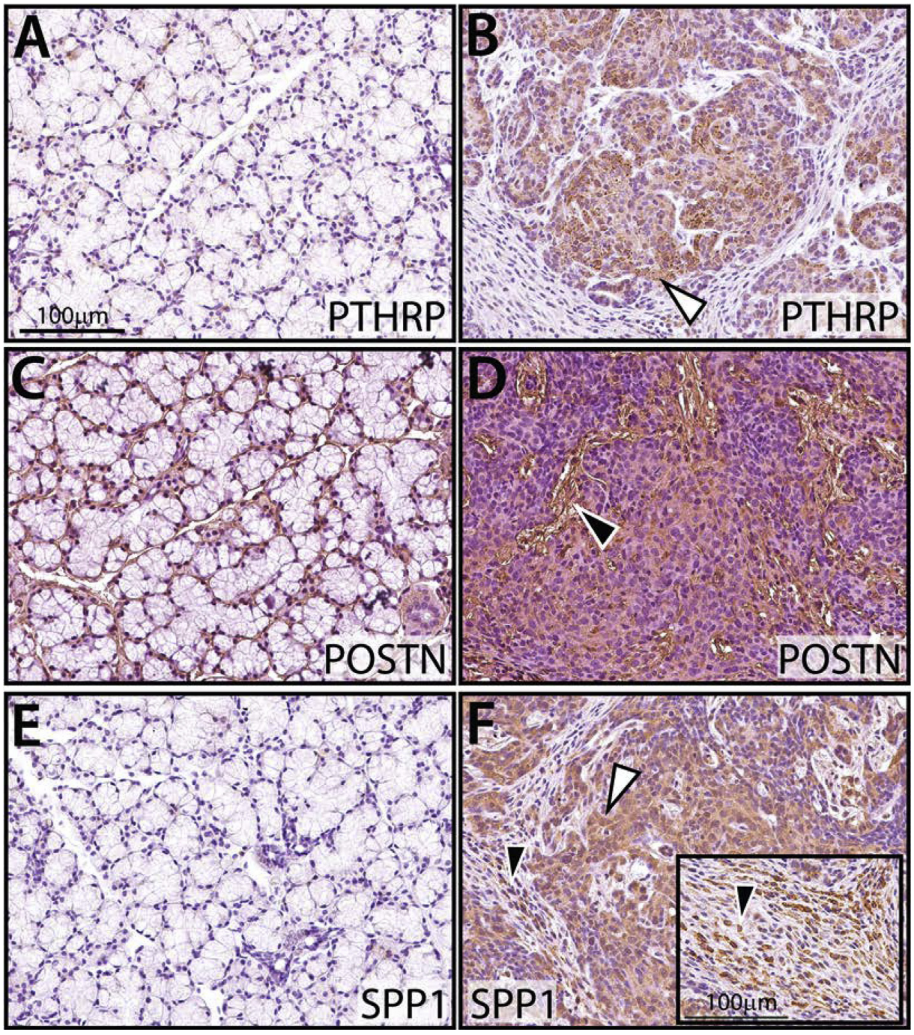

Fig. 7. The *K5:RANKL* salivary gland tumor expresses high levels of PTHRP, POSTN, and SPP1 protein. (A) and (B) Immunohistochemical staining for PTHRP in control salivary gland tissue and *K5:RANKL* salivary gland tumor tissue respectively. Note the conspicuous expression of PTHRP (white arrowhead) in the *K5:RANKL* tumor tissue compared to control. (C) and (D) Immunohistochemical detection of POSTN in control salivary gland tissue and *K5:RANKL* salivary gland tumor tissue respectively. While there are low levels of POSTN expression in control salivary gland tissue, note the marked increase in POSTN expression in the extracellular matrix of the *K5:RANKL* salivary gland tumor tissue (black arrowhead). (E) and (F) Immunohistochemical staining for SPP1 in control salivary gland tissue and *K5:RANKL* salivary gland tumor tissue respectively. Note the prominent expression of SPP1 in the epithelial (white arrowhead) and stromal (black arrowhead) compartments of the *K5:RANKL* salivary gland tumor tissue (inset shows a higher magnification of the stroma area that expresses SPP1 (black arrowhead)). Scale bars indicate 100 μm (scale bar in (A) applies to (B-F (excluding the inset)).

communication, migration, and signaling to the extracellular matrix or tumor microenvironment. These transcriptional programs are reflective of an aggressive tumor phenotype, with potential for locoregional invasion and distant metastasis. Through cross-species analysis, we showed that the transcriptomic signature of the *K5:RANKL* salivary gland tumor is most closely related to mesenchymal/basal subtypes of human head neck squamous cell carcinomas; mucoepidermoid carcinomas are not profiled by TCGA. Lending strong translational support for our mouse studies, the genes stratified in this analysis represent evolutionary conserved molecular targets that may prove important in the development of new molecular diagnostics and/or therapeutics in the future clinical management of salivary gland malignancies. As a corollary, the *K5:RANKL* transcriptomic dataset is also closely related to the human kidney renal clear cell carcinoma signature (Fig. 5A (KIRC)). This finding is interesting as RANKL/RANK signaling has recently been linked to poor prognosis in patients diagnosed with renal clear cell carcinoma [61] and supports the *K5:RANKL* transcriptomic signature as a powerful informational resource with which to molecularly understand RANKL-dependent cancers outside the head and neck cancer group.

In addition to RNA expression, we validated at the protein level the upregulation of three of these genes (PTHRP; POSTN; and SPP1) in the *K5:RANKL* salivary gland tumor. Apart from its role in humoral hypercalcemia and bone resorption [62], PTHRP is implicated in promoting metastasis of oral squamous cell carcinomas to bone [63–65]. Furthermore, studies support a role for PTHRP in conferring malignant potential to human mucoepidermoid carcinomas of the head and neck region [66], suggesting that PTHRP may be used as a prognostic factor for this malignancy type. Interestingly, previous studies have shown a close correlation between PTHRP and RANKL expression in a number of cancers [67–70], particularly in oral cancers that invade bone [70–73]. A secreted extracellular matrix protein, POSTN overexpression is also known as a prognostic indicator of poor survival for many cancers [74], including head and neck cancers [75–79]. An extracellular matrix protein, SPP1 is involved in tumor cell proliferation, invasion, and chemoresistance metastasis in a number of cancer types, such as nasopharyngeal and esophageal malignancies [80–82]. Taken together, our immunohistochemical analysis reinforces the robustness of the *K5:RANKL* salivary gland tumor model with which to study both established and novel oncogenic drivers of human salivary gland tumorigenesis in an *in vivo* context.

Apart from providing a new genome-wide transcriptomic resource to gain better insight into the key molecular mechanisms that drive development and progression of this understudied salivary gland malignancy, further mining of this resource may reveal novel molecular vulnerabilities that could be exploited for future targeted therapies. In future studies, the *K5:RANKL* mouse will be used to determine whether RANKL-dependent enlargement and activation of the cancer stem cell population drives the development of this tumor-type and whether these tumor cells exhibit intrinsic metastatic potential. Noteworthy, enlargement and intrinsic activation of the cancer stem cell population by RANKL has been shown to be a common cellular underpinning for the development and metastatic properties of other glandular tissue cancers such as the mammary gland [83]. Finally, the *K5:RANKL* mouse

represents an attractive preclinical *in vivo* model with which to assess the preventative and/or treatment efficacies of RANKL inhibitors in combination with other anti-neoplastic agents in the clinical management of this malignant neoplasm.

Acknowledgements

The authors thank Jie Li, Yan Ying, and Rong Zhao for their invaluable technical assistance in these studies. The technical services of the Mouse Embryonic Stem Cell, Genetically Engineered Mouse, Human Tissue Acquisition and Pathology Cores as well as the Genomic & RNA Profiling core at Baylor College of Medicine are acknowledged. These cores were funded by NIH P30 Cancer Center Support Grant (NCI-P30 CA125123), the P30 Digestive Disease Center Support Grant (NIDDK-DK56338), and the Knockout Mouse Project KOMP3 Grant (U42HG006352). For initial bioinformatic support, we thank Dr. Qianxing Mo at the Department of Medicine and Dan L. Duncan Cancer Center at Baylor College of Medicine. This research was also supported in part by Cancer Prevention & Research Institute of Texas (CPRIT: RP170005) to KR and CC, and by the National Institutes of Health (NIH)/National Institute of Child Health and Human Development (NICHD) grant: HD-042311 to JPL.

Declaration of Competing Interest

The authors declare that they have no conflict of interest concerning the studies described herein.

Authors' contributions

LH, MS, DL, and JL designed the studies and wrote the manuscript. LH and MS conducted the experiments. MI (a trained clinical pathologist) performed the histopathology analysis of *K5:RANKL* tumor samples and reviewed the manuscript. RF was involved in generating the transgenic mouse model. MS, KR, DP, and CC performed the bioinformatic analysis of the RNA-seq data.

Appendix A. Supplementary material

Supplementary data to this article can be found online at https://doi.org/10.1016/j.cyto.2019.154745.

References

[1] H. Boukheris, R.E. Curtis, C.E. Land, G.M. Dores, Incidence of carcinoma of the major salivary glands according to the WHO classification, 1992 to 2006: a population-based study in the United States, Cancer Epidemiol Biomarkers Prev 18 (2009) 2899–2906.
[2] G. Andry, M. Hamoir, L.D. Locati, L. Licitra, J.A. Langendijk, Management of salivary gland tumors, Expert Rev. Anticancer Ther. 12 (2012) 1161–1168.
[3] E. Barnes, J. Eveson, P. Reichart, World Health Organization classification of tumours: pathology and genetics of head and neck in tumours, IARCpress, Lyon, 2005.
[4] S.R. Chandana, B.A. Conley, Salivary gland cancers: current treatments, molecular characteristics and new therapies, Expert Rev. Anticancer Ther. 8 (2008) 645–652.
[5] J.A. Langendijk, P. Doornaert, I.M. Verdonck-de Leeuw, C.R. Leemans, N.K. Aaronson, B.J. Slotman, Impact of late treatment-related toxicity on quality of life among patients with head and neck cancer treated with radiotherapy, J. Clin. Oncol. 26 (2008) 3770–3776.
[6] J.J. Sciubba, D. Goldenberg, Oral complications of radiotherapy, Lancet Oncol. 7 (2006) 175–183.
[7] A. Vissink, J. Jansma, F.K. Spijkervet, F.R. Burlage, R.P. Coppes, Oral sequelae of head and neck radiotherapy, Crit. Rev. Oral Biol. Med. 14 (2003) 199–212.
[8] S.A. Laurie, L. Licitra, Systemic therapy in the palliative management of advanced salivary gland cancers, J. Clin. Oncol. 24 (2006) 2673–2678.
[9] M.R. Posner, T.J. Ervin, R.R. Weichselbaum, R.L. Fabian, D. Miller, Chemotherapy of advanced salivary gland neoplasms, Cancer 50 (1982) 2261–2264.
[10] D. Bell, E.Y. Hanna, Salivary gland cancers: biology and molecular targets for therapy, Curr. Oncol. Rep. 14 (2012) 166–174.
[11] J. Carlson, L. Licitra, L. Locati, D. Raben, F. Persson, G. Stenman, Salivary gland cancer: an update on present and emerging therapies, Am. Soc. Clin. Oncol. Educ. Book (2013) 257–263.
[12] A.R. Razak, L.L. Siu, C. Le Tourneau, Molecular targeted therapies in all histologies of head and neck cancers: an update, Curr. Opin. Oncol. 22 (2010) 212–220.
[13] S.G. Surakanti, M. Agulnik, Salivary gland malignancies: the role for chemotherapy and molecular targeted agents, Semin. Oncol. 35 (2008) 309–319.
[14] W.C. Dougall, M. Chaisson, The RANK/RANKL/OPG triad in cancer-induced bone diseases, Cancer Metastasis Rev. 25 (2006) 541–549.
[15] R. Fernandez-Valdivia, J.P. Lydon, From the ranks of mammary progesterone mediators, RANKL takes the spotlight, Mol. Cell. Endocrinol. 357 (2012) 91–100.
[16] M.C. Walsh, Y. Choi, Biology of the RANKL-RANK-OPG System in Immunity, Bone, and Beyond, Front. Immunol. 5 (2014) 511.
[17] T. Nakashima, Y. Kobayashi, S. Yamasaki, A. Kawakami, K. Eguchi, H. Sasaki, et al., Protein expression and functional difference of membrane-bound and soluble receptor activator of NF-kappaB ligand: modulation of the expression by osteotropic factors and cytokines, Biochem. Biophys. Res. Commun. 275 (2000) 768–775.
[18] L. Galibert, M.E. Tometsko, D.M. Anderson, D. Cosman, W.C. Dougall, The involvement of multiple tumor necrosis factor receptor (TNFR)-associated factors in the signaling mechanisms of receptor activator of NF-kappaB, a member of the TNFR superfamily, J. Biol. Chem. 273 (1998) 34120–34127.
[19] S. Rao, S.J.F. Cronin, V. Sigl, J.M. Penninger, RANKL and RANK: from mammalian physiology to cancer treatment, Trends Cell Biol. 28 (2018) 213–223.
[20] C.M. Bayer, M.W. Beckmann, P.A. Fasching, Updates on the role of receptor activator of nuclear factor kappaB/receptor activator of nuclear factor kappaB ligand/osteoprotegerin pathway in breast cancer risk and treatment, Curr. Opin. Obstet. Gynecol. 29 (2017) 4–11.
[21] M. Sisay, G. Mengistu, D. Edessa, The RANK/RANKL/OPG system in tumorigenesis and metastasis of cancer stem cell: potential targets for anticancer therapy, Onco Targets Ther 10 (2017) 3801–3810.
[22] M.S. Epstein, H.D. Ephros, J.B. Epstein, Review of current literature and implications of RANKL inhibitors for oral health care providers, Oral Surg. Oral Med. Oral Pathol. Oral Radiol. 116 (2013) e437–442.
[23] H. Furuta, K. Osawa, M. Shin, A. Ishikawa, K. Matsuo, M. Khan, et al., Selective inhibition of NF-kappaB suppresses bone invasion by oral squamous cell carcinoma in vivo, Int. J. Cancer 131 (2012) E625–635.
[24] M. Grimm, C. Renz, A. Munz, S. Hoefert, M. Krimmel, S. Reinert, Co-expression of CD44+/RANKL+ tumor cells in the carcinogenesis of oral squamous cell carcinoma, Odontology 103 (2015) 36–49.
[25] E. Jimi, M. Shin, H. Furuta, Y. Tada, J. Kusukawa, The RANKL/RANK system as a therapeutic target for bone invasion by oral squamous cell carcinoma (Review), Int. J. Oncol. 42 (2013) 803–809.
[26] Y. Sambandam, P. Ethiraj, J. Hathway-Schrader, C. Novince, E. Panneerselvam, K. Sundaram, et al., Autoregulation of RANK ligand in oral squamous cell carcinoma tumor cells, J. Cell. Physiol. (2018).
[27] Y. Sambandam, S. Sakamuri, S. Balasubramanian, A. Haque, RANK Ligand modulation of autophagy in oral squamous cell carcinoma tumor cells, J. Cell. Biochem. 117 (2016) 118–125.
[28] Y. Sambandam, K. Sundaram, A. Liu, K.L. Kirkwood, W.L. Ries, S.V. Reddy, CXCL13 activation of c-Myc induces RANK ligand expression in stromal/preosteoblast cells in the oral squamous cell carcinoma tumor-bone microenvironment, Oncogene 32 (2013) 97–105.
[29] K. Sato, J.W. Lee, K. Sakamoto, T. Iimura, K. Kayamori, H. Yasuda, et al., RANKL synthesized by both stromal cells and cancer cells plays a crucial role in osteoclastic bone resorption induced by oral cancer, Am. J. Pathol. 182 (2013) 1890–1899.
[30] M. Shin, K. Matsuo, T. Tada, H. Fukushima, H. Furuta, S. Ozeki, et al., The inhibition of RANKL/RANK signaling by osteoprotegerin suppresses bone invasion by oral squamous cell carcinoma cells, Carcinogenesis 32 (2011) 1634–1640.
[31] X. Zhang, C.R. Junior, M. Liu, F. Li, N.J. D'Silva, K.L. Kirkwood, Oral squamous carcinoma cells secrete RANKL directly supporting osteolytic bone loss, Oral Oncol. 49 (2013) 119–128.
[32] M.L. Blake, M. Tometsko, R. Miller, J.C. Jones, W.C. Dougall, RANK expression on breast cancer cells promotes skeletal metastasis, Clin. Exp. Metastasis 31 (2014) 233–245.
[33] J.R. Canon, M. Roudier, R. Bryant, S. Morony, M. Stolina, P.J. Kostenuik, et al., Inhibition of RANKL blocks skeletal tumor progression and improves survival in a mouse model of breast cancer bone metastasis, Clin. Exp. Metastasis 25 (2008) 119–129.
[34] D.H. Jones, T. Nakashima, O.H. Sanchez, I. Kozieradzki, S.V. Komarova, I. Sarosi, et al., Regulation of cancer cell migration and bone metastasis by RANKL, Nature 440 (2006) 692–696.
[35] X. Li, Y. Liu, B. Wu, Z. Dong, Y. Wang, J. Lu, et al., Potential role of the OPG/RANK/RANKL axis in prostate cancer invasion and bone metastasis, Oncol. Rep. 32 (2014) 2605–2611.
[36] A. Franchi, C. Taverna, A. Simoni, M. Pepi, G. Mannelli, M. Fasolati, et al., RANK and RANK ligand expression in parotid gland carcinomas, Appl. Immunohistochem. Mol. Morphol. (2018).
[37] J. Eveson, Tumors of the salivary glands, in: L. Barnes, D. Sidransky (Eds.), World Health Organization Classification of Tumours: Pathology & Genetics of Head and Neck Tumours, IARC, 2005, pp. 209–281.
[38] R.R. Seethala, An update on grading of salivary gland carcinomas, Head Neck Pathol 3 (2009) 69–77.
[39] G. Seifert, L. Sobin, Histological typing of salivary gland tumors (WHO. World Health Organization), Second ed., Berlin, Springer-Verlag, 1991.
[40] R.K. Goode, P.L. Auclair, G.L. Ellis, Mucoepidermoid carcinoma of the major salivary glands: clinical and histopathologic analysis of 234 cases with evaluation of grading criteria, Cancer 82 (1998) 1217–1224.
[41] M.A. Luna, Salivary mucoepidermoid carcinoma: revisited, Adv Anat Pathol 13 (2006) 293–307.
[42] M.M. Szwarc, R. Kommagani, A.P. Jacob, W.C. Dougall, M.M. Ittmann, J.P. Lydon,

Aberrant activation of the RANK signaling receptor induces murine salivary gland tumors, PLoS ONE 10 (2015) e0128467.
[43] A.R. Raimondi, L. Vitale-Cross, P. Amornphimoltham, J.S. Gutkind, A. Molinolo, Rapid development of salivary gland carcinomas upon conditional expression of K-ras driven by the cytokeratin 5 promoter, Am. J. Pathol. 168 (2006) 1654–1665.
[44] L. Vitale-Cross, P. Amornphimoltham, G. Fisher, A.A. Molinolo, J.S. Gutkind, Conditional expression of K-ras in an epithelial compartment that includes the stem cells is sufficient to promote squamous cell carcinogenesis, Cancer Res. 64 (2004) 8804–8807.
[45] A. Mukherjee, S.M. Soyal, J. Li, Y. Ying, B. He, F.J. DeMayo, et al., Targeting RANKL to a specific subset of murine mammary epithelial cells induces ordered branching morphogenesis and alveologenesis in the absence of progesterone receptor expression, FASEB J. 24 (2010) 4408–4419.
[46] A. Mukherjee, S.M. Soyal, J. Li, Y. Ying, M.M. Szwarc, B. He, et al., A mouse transgenic approach to induce beta-catenin signaling in a temporally controlled manner, Transgenic Res. 20 (2011) 827–840.
[47] M.M. Szwarc, R. Kommagani, M.C. Peavey, L. Hai, D.M. Lonard, J.P. Lydon, A bioluminescence reporter mouse that monitors expression of constitutively active beta-catenin, PLoS ONE 12 (2017) e0173014.
[48] M.M. Szwarc, L. Hai, W.E. Gibbons, M.C. Peavey, L.D. White, Q. Mo, et al., Human endometrial stromal cell decidualization requires transcriptional reprogramming by PLZF, Biol. Reprod. 98 (2018) 15–27.
[49] A. Dobin, C.A. Davis, F. Schlesinger, J. Drenkow, C. Zaleski, S. Jha, et al., STAR: ultrafast universal RNA-seq aligner, Bioinformatics 29 (2013) 15–21.
[50] M.I. Love, W. Huber, S. Anders, Moderated estimation of fold change and dispersion for RNA-seq data with DESeq2, Genome Biol. 15 (2014) 550.
[51] Y. Benjamini, Y. Hochberg, Controlling the false discovery rate: a practical and powerful approach to multiple testing, J. Royal Statistical Soc. Series B (Methodological) 57 (1995) 289–300.
[52] S. Lindgreen, AdapterRemoval: easy cleaning of next-generation sequencing reads, BMC Res Notes 5 (2012) 337.
[53] M. Pertea, D. Kim, G.M. Pertea, J.T. Leek, S.L. Salzberg, Transcript-level expression analysis of RNA-seq experiments with HISAT, StringTie and Ballgown, Nat. Protoc. 11 (2016) 1650–1667.
[54] A. Frankish, B. Uszczynska, G.R. Ritchie, J.M. Gonzalez, D. Pervouchine, R. Petryszak, et al., Comparison of GENCODE and RefSeq gene annotation and the impact of reference geneset on variant effect prediction, BMC Genomics 16 (Suppl 8) (2015) S2.
[55] V. Chitsazzadeh, C. Coarfa, J.A. Drummond, T. Nguyen, A. Joseph, S. Chilukuri, et al., Cross-species identification of genomic drivers of squamous cell carcinoma development across preneoplastic intermediates, Nat. Commun. 7 (2016) 12601.
[56] M. Krzywinski, J. Schein, I. Birol, J. Connors, R. Gascoyne, D. Horsman, et al., Circos: an information aesthetic for comparative genomics, Genome Res. 19 (2009) 1639–1645.
[57] R.H. Spiro, A.G. Huvos, R. Berk, E.W. Strong, Mucoepidermoid carcinoma of salivary gland origin. a clinicopathologic study of 367 cases, Am. J. Surg. 136 (1978) 461–468.
[58] D.M. Guimaraes, L.O. Almeida, M.D. Martins, K.A. Warner, A.R. Silva, P.A. Vargas, et al., Sensitizing mucoepidermoid carcinomas to chemotherapy by targeted disruption of cancer stem cells, Oncotarget 7 (2016) 42447–42460.
[59] A. Lagha, N. Chraiet, M. Ayadi, S. Krimi, B. Allani, H. Rifi, et al., Systemic therapy in the management of metastatic or advanced salivary gland cancers, Oral Oncol. 48 (2012) 948–957.
[60] V.P. Wagner, M.A. Martins, M.D. Martins, K.A. Warner, L.P. Webber, C.H. Squarize, et al., Overcoming adaptive resistance in mucoepidermoid carcinoma through inhibition of the IKK-beta/IkappaBalpha/NFkappaB axis, Oncotarget 7 (2016) 73032–73044.
[61] A. Steven, S. Leisz, S. Fussek, B. Nowroozizadeh, J. Huang, D. Branstetter, et al., Receptor activator of NF-kappaB (RANK)-mediated induction of metastatic spread and association with poor prognosis in renal cell carcinoma, Urol Oncol. (2018).
[62] J.J. Wysolmerski, Parathyroid hormone-related protein: an update, J. Clin. Endocrinol. Metab. 97 (2012) 2947–2956.
[63] Z. Lv, X. Wu, W. Cao, Z. Shen, L. Wang, F. Xie, et al., Parathyroid hormone-related protein serves as a prognostic indicator in oral squamous cell carcinoma, J. Exp. Clin. Cancer Res. 33 (2014) 100.
[64] S. Sen, P. Dasgupta, G. Kamath, H.S. Srikanth, Paratharmone related protein (peptide): a novel prognostic, diagnostic and therapeutic marker in head & neck cancer, J Stomatol Oral Maxillofac Surg 119 (2018) 33–36.
[65] Y. Takayama, T. Mori, T. Nomura, T. Shibahara, M. Sakamoto, Parathyroid-related protein plays a critical role in bone invasion by oral squamous cell carcinoma, Int. J. Oncol. 36 (2010) 1387–1394.
[66] K. Nagamine, T. Kitamura, A. Yanagawa-Matsuda, Y. Ohiro, K. Tei, K. Hida, et al., Expression of parathyroid hormone-related protein confers malignant potential to mucoepidermoid carcinoma, Oncol. Rep. 29 (2013) 2114–2118.
[67] H. Kumamoto, K. Ooya, Expression of parathyroid hormone-related protein (PTHrP), osteoclast differentiation factor (ODF)/receptor activator of nuclear factor-kappaB ligand (RANKL) and osteoclastogenesis inhibitory factor (OCIF)/osteoprotegerin (OPG) in ameloblastomas, J. Oral Pathol. Med. 33 (2004) 46–52.
[68] F.C. Perez-Martinez, V. Alonso, J.L. Sarasa, F. Manzarbeitia, R. Vela-Navarrete, F.J. Calahorra, et al., Receptor activator of nuclear factor-kappaB ligand (RANKL) as a novel prognostic marker in prostate carcinoma, Histol. Histopathol. 23 (2008) 709–715.
[69] J.C. Zong, X. Wang, X. Zhou, C. Wang, L. Chen, L.J. Yin, et al., Gut-derived serotonin induced by depression promotes breast cancer bone metastasis through the RUNX2/PTHrP/RANKL pathway in mice, Oncol. Rep. 35 (2016) 739–748.
[70] R.W. Cowan, G. Singh, M. Ghert, PTHrP increases RANKL expression by stromal cells from giant cell tumor of bone, J. Orthop. Res. 30 (2012) 877–884.
[71] N. Cui, T. Nomura, N. Takano, E. Wang, W. Zhang, T. Onda, et al., Osteoclast-related cytokines from biopsy specimens predict mandibular invasion by oral squamous cell carcinomas, Exp Ther Med 1 (2010) 755–760.
[72] E. Jimi, H. Furuta, K. Matsuo, K. Tominaga, T. Takahashi, O. Nakanishi, The cellular and molecular mechanisms of bone invasion by oral squamous cell carcinoma, Oral Dis. 17 (2011) 462–468.
[73] F.C. Perez-Martinez, V. Alonso, J.L. Sarasa, S.G. Nam-Cha, R. Vela-Navarrete, F. Manzarbeitia, et al., Immunohistochemical analysis of low-grade and high-grade prostate carcinoma: relative changes of parathyroid hormone-related protein and its parathyroid hormone 1 receptor, osteoprotegerin and receptor activator of nuclear factor-kB ligand, J. Clin. Pathol. 60 (2007) 290–294.
[74] L. Gonzalez-Gonzalez, J. Alonso, Periostin: a matricellular protein with multiple functions in cancer development and progression, Front. Oncol. 8 (2018) 225.
[75] Y. Kudo, I. Ogawa, S. Kitajima, M. Kitagawa, H. Kawai, P.M. Gaffney, et al., Periostin promotes invasion and anchorage-independent growth in the metastatic process of head and neck cancer, Cancer Res. 66 (2006) 6928–6935.
[76] M. Li, C. Li, D. Li, Y. Xie, J. Shi, G. Li, et al., Periostin, a stroma-associated protein, correlates with tumor invasiveness and progression in nasopharyngeal carcinoma, Clin. Exp. Metastasis 29 (2012) 865–877.
[77] C.Z. Michaylira, G.S. Wong, C.G. Miller, C.M. Gutierrez, H. Nakagawa, R. Hammond, et al., Periostin, a cell adhesion molecule, facilitates invasion in the tumor microenvironment and annotates a novel tumor-invasive signature in esophageal cancer, Cancer Res. 70 (2010) 5281–5292.
[78] X. Qin, M. Yan, J. Zhang, X. Wang, Z. Shen, Z. Lv, et al., TGFbeta3-mediated induction of Periostin facilitates head and neck cancer growth and is associated with metastasis, Sci. Rep. 6 (2016) 20587.
[79] T.J. Underwood, A.L. Hayden, M. Derouet, E. Garcia, F. Noble, M.J. White, et al., Cancer-associated fibroblasts predict poor outcome and promote periostin-dependent invasion in oesophageal adenocarcinoma, J. Pathol. 235 (2015) 466–477.
[80] A. Celetti, D. Testa, S. Staibano, F. Merolla, V. Guarino, M.D. Castellone, et al., Overexpression of the cytokine osteopontin identifies aggressive laryngeal squamous cell carcinomas and enhances carcinoma cell proliferation and invasiveness, Clin. Cancer Res. 11 (2005) 8019–8027.
[81] Q.T. Le, P.D. Sutphin, S. Raychaudhuri, S.C. Yu, D.J. Terris, H.S. Lin, et al., Identification of osteopontin as a prognostic plasma marker for head and neck squamous cell carcinomas, Clin. Cancer Res. 9 (2003) 59–67.
[82] J. Lin, A.L. Myers, Z. Wang, D.J. Nancarrow, D. Ferrer-Torres, A. Handlogten, et al., Osteopontin (OPN/SPP1) isoforms collectively enhance tumor cell invasion and dissemination in esophageal adenocarcinoma, Oncotarget 6 (2015) 22239–22257.
[83] M. Palafox, I. Ferrer, P. Pellegrini, S. Vila, S. Hernandez-Ortega, A. Urruticoechea, et al., RANK induces epithelial-mesenchymal transition and stemness in human mammary epithelial cells and promotes tumorigenesis and metastasis, Cancer Res. 72 (2012) 2879–2888.